

Single-cycle attosecond pulses by Thomson backscattering of terahertz pulses

György Tóth^{1,2,*}, Zoltán Tibai¹, Ashutosh Sharma³, József A. Fülöp^{2,3,4}, and János Hebling^{1,2,4}

¹Institute of physics, University of Pécs, 7624 Pécs, Hungary

²MTA-PTE High-Field Terahertz Research Group, 7624 Pécs, Hungary

³ELI-ALPS, ELI-Hu Nkft., 6720 Szeged, Hungary

⁴Szentágotthai Research Centre, University of Pécs, 7624 Pécs, Hungary

March 13, 2022

Abstract

The generation of single-cycle attosecond pulses based on Thomson scattering of terahertz (THz) pulses is proposed. In the scheme, a high-quality relativistic electron beam produced by a laser-plasma wakefield accelerator (LPWA), is sent through suitable magnetic devices to produce ultrathin electron layers for coherent Thomson backscattering of intense THz pulses. According to numerical simulations, single-cycle attosecond pulse generation is possible with up to 1 nJ energy. The waveform of the attosecond pulses closely resembles that of the THz pulses. This allows for a flexible waveform control of attosecond pulses.

1 Introduction

Attosecond pulses can be generated in a number of ways, such as high-harmonic generation [1], undulator radiation [2–5], or Thomson scattering [6–9]. High-harmonic generation is capable of producing single-cycle attosecond pulses [10]. Even subcycle pulses were generated by laser-generated ultrathin electron layers from double-foil targets [11]. However, controlling the pulse shape has not been demonstrated so far. This is also true of radiation sources based on relativistic electrons [5, 12]. In order to circumvent this limitation, we proposed a technique to generate carrier-envelope phase stable, waveform-controlled single-cycle [13, 14] or few-cycle [15] attosecond pulses by coherent undulator radiation. In this scheme, ultrathin (of a few nm) relativistic electron layers, generated in a laser-assisted bunching process, emit attosecond pulses when passing through a radiator undulator. The magnetic field distribution of the undulator is transferred to the waveform of the emitted radiation [13–15], thereby offering a unique waveform tailoring capability. Nevertheless, this technique requires high-energy

(GeV) electrons, as an extremely short undulator would be necessary for lower-energy (<100 MeV) electrons, which are more easily available even from laser electron accelerators.

A LPWA is able to generate electron beams over cm acceleration distances with parameters comparable to (and in some regards even better than) conventional sources. The pulse duration unique to LPWAs is intrinsically ultrashort, which is more than one order of magnitude shorter than those in X-ray free electron lasers (XFELs). The recent progresses in LPWA [16–18] allow efficient production of high quality electron beams in very high electric fields, moreover it has opened the possibility to design and conceive the compact setup [19].

Alternatively, Thomson scattering is capable to generate attosecond pulses from low-energy electrons (see e.g. [7]). Single-cycle attosecond pulse generation by Thomson scattering is possible using single-cycle laser pulses. However, single-cycle laser pulse generation is a big challenge in the visible spectral range. Therefore, alternative methods can be of significant interest.

In this paper, we propose a setup to generate waveform-controlled single-cycle attosecond pulses by Thomson scattering of intense THz pulses. In the terahertz (THz) spectral range, single-cycle pulse generation is straightforward [20–24]. The peak electric field of the most intense THz pulses today reaches 40 MV/cm [22], and there are many suggestions to increase the efficiency of THz generation [25–29]. Here, we show that such THz pulses are a useful tool in generating single-cycle or waveform controlled attosecond pulses by Thomson scattering on 30–40 MeV electrons, conveniently delivered by present laser-driven electron sources.

The paper is organized as follows. Section 2 describes the basics of Thomson scattering. Section 3 introduces the setup proposed in this work. Section 4 describes the calculation method. The results and their discussion are presented in Section 5. The conclusion is drawn in the last section.

2 Scheme of the attosecond source

The proposed setup for the generation of single-cycle attosecond pulses is shown in Fig 1. Relativistic electrons are generated in a LPWA. The electron beam is propagated through the first triplet of quadrupoles to reduce the divergence of the beam. However, the typical energy spread of a LPWA beam is of a few percent. Importantly, the slice energy spread can be reduced by a chicane. The second triplet of quadrupoles focuses the electron beam to the focus of the THz radiation. In order to generate a spatially periodic energy modulation of the electrons, a high-power laser pulse is superimposed on them in the modulator undulator (MU). This energy modulation leads to the formation of ultrathin (<20 nm) electron layers (nanobunches) in the drift space behind the MU. A counterpropagating strong-field THz pulse is focused to the position where the nanobunch has the smallest longitudinal size, where the electrons interact with the THz field.

Advantageously, a single laser system is used to drive the attosecond source, including the electron source, the nanobunching, and the THz source. A short-pulse pumped high-power few-cycle optical parametric chirped-pulse amplification (OPCPA) system can be an ideally fitting laser architecture [30–32]. Whereas the 10 to 100-TW power OPCPA output pulses are suitable to drive

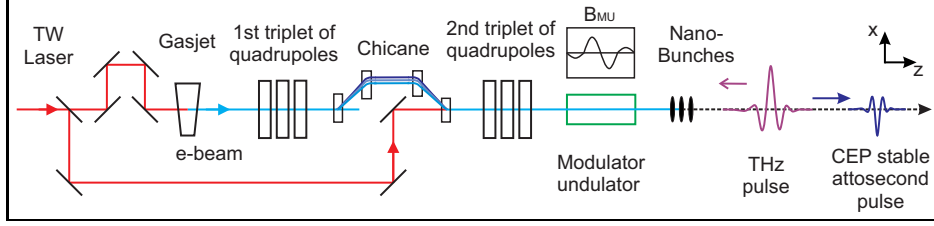


Figure 1: Scheme of the proposed LPWA-based, THz-driven Thomson scattering setup for singlecycle attosecond pulse generation.

the LPWA and the nanobunching, the sub-ps to few-ps pump pulses can be used to efficiently drive the THz source.

3 Simulation methods

The simulation consists of two main parts. Firstly, we calculated a LPWA process, the transport and manipulation of the electron bunch, including nanobunch generation. Secondly, Thomson-scattering was calculated with the initial electron bunch parameters from the first part.

3.1 Generation and manipulation of relativistic electrons

In order to create a coherent attosecond source, a good quality electron beam with high charge and few tens of MeV energy is needed. According to the scaling law predicted by Gordienko and Pukhov [33], a high quality electron beam can be generated in the bubble regime by utilizing laser pulses with 800 nm central wavelength, a pulse duration of 8 fs, and 80 mJ pulse energy, corresponding to 10 TW power. Such a laser pulse can be focused in gas target to an optimized spot size of $3.7 \mu\text{m}$ corresponding to a peak intensity of $2.9 \times 10^{19} \text{ W/cm}^2$. As per scaling the optimum density range for efficient electron acceleration in bubble regime can be estimated as $1.5 \times 10^{19} \text{ cm}^{-3}$. Following the mentioned scaling law [33], an electron beam of 34 MeV energy and 442 pC charge can be obtained in an acceleration distance of $78 \mu\text{m}$. The main parameters of the used electron beam are listed in Table 1.

Table 1: **Parameters of the electron beam from the LPWA.**

Parameter	Value
Energy (γ_0)	68
Energy spread (σ_{γ_0})	2 %
Normalized emittance ($\gamma_0 \varepsilon_{x,y}$)	0.078 mm mrad
Transversal size ($\sigma_{x0} = \sigma_{y0}$)	$5 \mu\text{m}$
Length (σ_{z0})	$5 \mu\text{m}$
Charge	442 pC

The General Particle Tracer (GPT) numerical code was used for the simulation of the electron beam transport and the ultrathin electron layer generation. One million macroparticles were used in the calculation, whereby one macroparticle consisted of 2760 electrons. The electron beam from a LPWA typically

has a large transversal divergence, the reduction of which is important for further use. Furthermore, it was shown that the generation of coherent radiation is more efficient, when the transversal size of the nanobunch is smaller [13]. Therefore, the electron beam was focused by two quadrupole triplets to the THz beam waist. The gradients of the quadrupole triplets were optimized with a self-developed numerical code. In the best case 15 μm and 25 μm transversal sizes were calculated in the x and y directions, respectively. The first chicane decompresses the electron bunch longitudinally, and after the chicane the slice energy spread of the electron bunch is reduced from 2 % to 0.2 %. The main parameters of the quadrupoles and the chicane are listed in Table 2.

Table 2: **Parameters of the quadrupoles and the chicane.**

Parameter	Value
Distance between the gas jet and the 1st quadrupole triplet	15 cm
1st quadrupole triplet gradients	10.1/-7.1/3.2
1st quadrupole triplet elements length	10 cm
Chicane dipole strength	0.043 T
Chicane dipole length	15 cm
2nd quadrupole triplet gradients	-2.5/5.6/-6.2
2nd quadrupole triplet elements length	10 cm

The relativistic electron beam is sent through the modulator undulator (MU), where a 17-TW power laser beam of 800 nm central wavelength is superimposed on it, in order to generate nanobunches. The MU used here has two periods. The magnetic field of the MU is trimmed in antisymmetric design $(1/4, -3/4, 3/4, -1/4)$ along the electron propagation direction. After modulating the electron energy with the laser, a series of nanobunches is being formed. The individual nanobunches are separated by the modulator laser wavelength. The shortest nanobunch with only 16 nm length, containing a charge of 0.6 pC, was used in the simulation of Thomson scattering. The modulator laser and MU parameters are listed in Table 3. The spatial distribution of the nanobunch is shown in Fig. 2, where the color represents the energies of the macroparticles.

Table 3: **Parameters of the modulator laser and the modulator undulator.**

Parameter	Value
Laser wavelength (λ_l)	800 nm
Laser peak power	17 TW
Laser beam waist	1 mm
Laser beam Rayleigh length	3.9 m
MU undulator parameter (K_{MU})	0.5
MU period length (λ_{MU})	6.7 mm

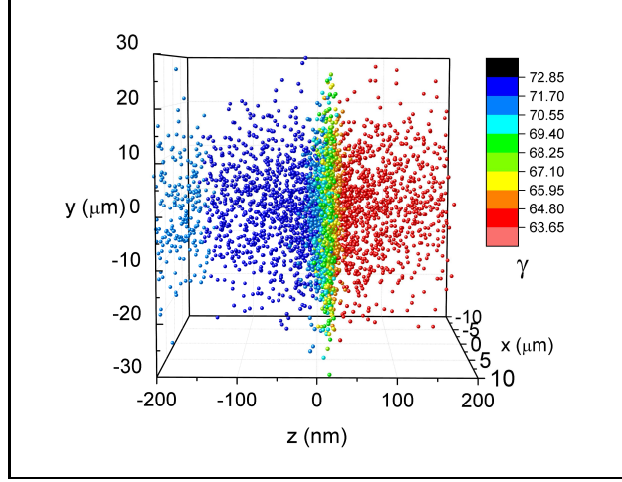


Figure 2: The spatial and energy distribution of macroparticles in our model. One sphere represents 2760 electrons. The energy distribution of macroparticles (together the real electrons) show the color scale.

3.2 Thomson scattering

The interaction of a thin layer of relativistic electrons with a counterpropagating intense THz pulse results in Thomson scattering, schematically shown in Fig. 3. During the interaction, the electromagnetic field of the THz pulse affects the movement of the electrons according to the Lorentz-law. The resulting oscillatory electron motion generates a radiation field, which can be determined based on Lienard-Wiecher potentials [34] as:

$$\vec{E}(\vec{r}, t) = \left[\frac{q_e \mu_0}{4\pi} \frac{\vec{R} \times \left(\left(\vec{R} - R\vec{\beta} \right) \times \frac{d}{dt} \vec{v} \right)}{\left(R - \vec{R} \cdot \vec{\beta} \right)^3} \right]_{ret}, \quad (1)$$

where q_e is the charge of the electron, μ_0 is the vacuum permeability, \vec{R} is the vector pointing from the position of the electron at the retarded moment to the observation point, \vec{v} is the velocity of the electron, $\vec{\beta} = \vec{v}/c$, and c is the speed of light.

When the THz pulse with λ_0 central wavelength interacts with a relativistic electron, the wavelength of the backscattered radiation field becomes [35]

$$\lambda_r = \frac{1 + a_0^2/2 + \gamma^2 \theta^2}{2(1 + \cos \phi)} \cdot \frac{\lambda_0}{\gamma^2}, \quad (2)$$

where $\gamma = \left(1 - v^2/c^2 \right)^{-1/2}$ is the relativistic factor of the electron, θ is the angle between the electron propagation direction and the observation axis, ϕ is the interaction angle between the THz pulse and the electron, and $a_0 = q_e E_0 / m_e c \omega_0$ is the normalized THz field strength, where E_0 is the peak electric field, $\omega_0 = 2\pi c / \lambda_0$ is the angular frequency, and m_e is the mass of the electron.

The scattered field was determined according to Eq. 1, whereby macroparticles, rather than single electrons, were taken into account. Accordingly, q_e and

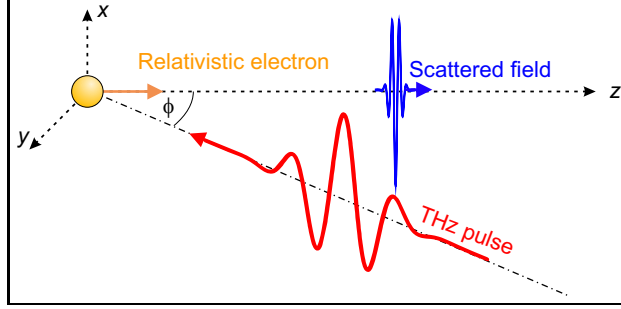


Figure 3: Scheme of Thomson scattering of a single-cycle THz pulse on relativistic electrons. Both the THz pulse as well as the scattered pulse are polarized along the x direction. The incoming THz pulse propagates in the yz plane.

m_e was equal to the charge and the mass of one macroparticle, respectively. In order to use Eq. 1, first it was necessary to solve the equation of motion for the macroparticles in the electromagnetic field of the THz pulse. The equation of motion reads as:

$$\frac{d\vec{p}}{dt} = q_0 \left(\vec{E}(\rho, z, t) + \vec{v}(t) \times \vec{B}(\rho, z, t) \right), \quad (3)$$

where $\vec{p} = m_0 \gamma \vec{v}$ is the electron momentum vector, m_0 is the mass of the macroparticle, q_0 is the charge of the macroparticle, ρ is the radial coordinate, t is the time. The electric and the magnetic fields of the THz pulse are given as follows, respectively:

$$\begin{aligned} \vec{E}(\rho, z, t) = E_0 \vec{x} \frac{w_0}{w(z)} \exp \left(-\frac{\rho^2}{w^2(z)} \right) \times \\ \exp \left(-2 \ln(2) \frac{(z/c + t)^2}{\tau^2} \right) \cos(k_0(z + ct) - \Psi(z)), \end{aligned} \quad (4)$$

$$\vec{B}(\rho, z, t) = \frac{1}{k_0 c} \vec{E}(\rho, z, t) \times \vec{k}_0. \quad (5)$$

In these equations, \vec{x} is the direction of the electric field polarization, w_0 is the THz beam waist radius, $w(z) = w_0 \sqrt{1 + \left(\frac{z}{z_R} \right)^2}$ is the beam radius at position z , $z_R = \frac{\pi w_0^2}{\lambda}$ is the Rayleigh length of the Gaussian beam, λ_0 is the central wavelength of the THz pulse, τ is the full width at half maximum (FWHM) of the intensity in time, $\vec{k}_0 = \frac{2\pi}{\lambda_0} \vec{e}_z$ is the wave vector, $\Psi(z) = \arctan \left(\frac{z}{z_R} \right)$ is the Gouy phase. Because single-cycle THz pulses were supposed, the FWHM of the pulses were $\tau = \frac{2\pi}{k_0 c}$.

The energy of the electromagnetic pulse in the vacuum can be calculated according to $W = \int_{-\infty}^{\infty} \int_0^{\pi} \int_0^{\infty} \frac{1}{2} \epsilon_0 c \left| \vec{E}(\rho, z, t) \right|^2 \rho d\rho d\phi dt$ [36], so the field amplitude in Eq. (4) was calculated as:

$$E_0 = \frac{2\sqrt{2} (\ln 2)^{\frac{1}{4}} \sqrt{W}}{\sqrt{\epsilon_0 c \pi^{\frac{3}{2}} \tau w_0}}, \quad (6)$$

where ϵ_0 is the vacuum permittivity.

For linear Thomson scattering, the total output radiation yield is proportional to the intensity of the THz pulse [35,37]. Therefore, the laser pulse must be focused to increase its intensity. In the calculations, $w_0 = c/\nu_0$ was assumed, where ν_0 is the central frequency of the THz pulse. Using this focusing and the single-cycle conditions, Eq. 6 gives the following energy- and frequency-dependent relationship:

$$E_0 = \frac{2\sqrt{2}(\ln 2)^{\frac{1}{4}}}{c\sqrt{\epsilon_0 c\pi^{\frac{3}{2}}}} \sqrt{W\nu_0^3}, \quad (7)$$

We note that in the calculations of the next Section, head-on collision between the electron and the THz beams was assumed and Eq. 2 can be simplified to:

$$\lambda_r = (1 + a_0^2/2 + \gamma^2\theta^2) \cdot \frac{\lambda_0}{4\gamma^2}. \quad (8)$$

4 Results and discussion

We investigated the dependence of the scattered field energy on the frequency and energy of the THz pulse. The results are shown in Fig. 4. In accordance with previous theoretical predictions for laser pulses [35,37], the radiated energy is proportional to the THz pulse energy. Therefore, the scattered radiation energy can be increased by increasing the energy of the THz pulse.

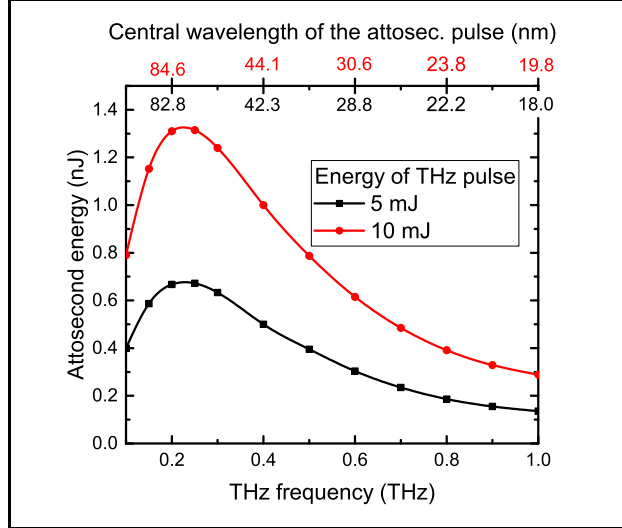


Figure 4: Energy of the generated single-cycle attosecond pulse as function of the central frequency of the THz pulse in case of 5 mJ (black curve) and 10 mJ (red curve) THz pulse energies. The upper axis shows the predicted central wavelength of the emitted radiation according to Eq. 2. Values in black (red) correspond to 5 mJ (10 mJ).

Figure 4 shows that the radiated energy, as function of the THz frequency, has a maximum at about 0.2 THz. The initial increase at lower THz frequencies

can be explained as follows. The number of radiated photons per electron in case of a single-cycle THz pulse is given by $N \approx \alpha \cdot a_0^2$ [38], where α is the fine structure constant. The THz pulse energy was kept constant along each curve in Fig. 4, whereby a single-cycle waveform and a diffraction-limited focal spot size was assumed at each value of the THz central frequency. The resulting $a_0^2 \propto W \times \nu_0$ scaling leads to $N \propto \nu_0$. In addition, the energy of the radiated photon also increases with the THz frequency (see Eq. 2). It means that the energy emitted by one electron increases with increasing ν_0 . As long as transversal effects can be neglected (see below), this leads to an increasing total emitted energy for an extended nanobunch.

However, as the THz frequency, and consequently the radiation frequency, increases, transversal effects for the extended electron sheet become significant. As we showed in [13], owing to coherent superposition, the solid angle of the emitted radiation for a nanobunch with a finite transversal size is smaller than that for a single electron. This also reduces the total radiated energy. Obviously, this effect becomes stronger for higher frequency (smaller wavelength) of the emitted radiation. This is the reason for the decreasing radiated energy with increasing THz frequency.

For a given THz frequency, the energy of the THz pulse is proportional to a_0^2 . Therefore, according to Eq. 2, increasing the THz energy at a constant THz frequency results in increasing radiation wavelength as $\lambda_r \propto 1 + a_0^2/2$ for $\theta = 0$. This, together with the $a_0^2 \propto W \times \nu_0$ scaling mentioned above, causes a moderate variation of the radiation wavelength with the THz energy. By increasing the THz energy from 5 mJ to 10 mJ leads to about 2% (10%) shift in the radiation wavelength at 0.1 THz (1 THz) frequency.

A comparison of incoming THz and scattered attosecond pulse waveforms and spectra are shown in Fig. 5.a and 5.b, respectively. In Fig. 5.a the red curve shows a single-cycle THz pulse with 10 mJ energy and 0.4 THz central frequency. The blue curve shows the scattered field. The two waveforms are very similar. The pulse duration of the scattered pulse is less than 150 as with 48 nm central wavelength, consistent with the single-cycle waveform. The central frequency of the scattered field is about 17,000 times higher than the THz frequency, in good agreement with Eq. 2. This is clearly shown in Fig. 5.b, where the blue curve shows the spectrum of the attosecond pulse and the red curve shows the spectrum of the THz pulse on a 17,000 times larger wavelength scale.

We note that varying the interaction angle ϕ between the propagation direction of the electrons and the propagation direction of the THz pulse (see Fig. 3) allows to use an electron bunch with still higher energy. For example, $\phi = 90^\circ$ allows for two times larger electron energy to be used. Because the radiated energy is proportional to the square of the electron energy, up to four times higher emitted pulse energy can be expected.

Furthermore, a tunable narrowband extreme ultraviolet source can also be constructed based on the proposed method, whereby a tunable THz source can be used. A suitable THz source can be a semiconductor contact-grating device [25], pumped by the periodically intensity-modulated pulses from a dual-chirped optical parametric amplifier [39].

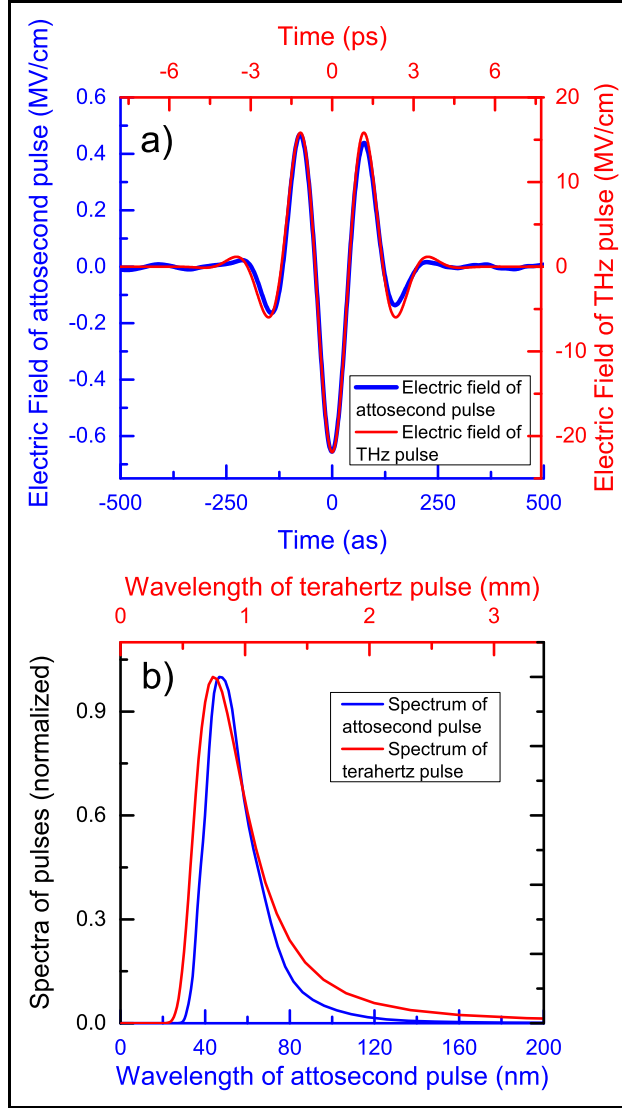


Figure 5: (a) The temporal waveforms of the Thomson-scattered pulse (blue) and the incoming THz pulse (red). (b) Spectra of the scattered field (blue) and the THz pulse (red).

5 Conclusion

A novel scheme of single-cycle attosecond pulse generation was introduced, and investigated by numerical simulations. The entirely laser-based scheme uses electrons of a few tens-of-MeV energy generated by a laser wakefield accelerator, subsequent nanobunching to ultrathin electron layers in a modulating undulator driven by TW laser pulses, and the Thomson scattering of intense THz pulses to generate nJ-level attosecond pulses in the few tens of nm wavelength range. The scheme can be driven for example by a short-pulse pumped few-cycle OPCPA system, whereby the strong THz pulses can be conveniently generated by the pump laser. The waveform of the generated attosecond pulses closely resembles that of the THz pulses and can be flexibly shaped by shaping the THz pulse.

References

- [1] Ferenc Krausz and Misha Ivanov. Attosecond physics. *Rev. Mod. Phys.*, 81:163–234, Feb 2009.
- [2] Alexander A Zholents and William M Fawley. Proposal for intense attosecond radiation from an x-ray free-electron laser. *Phys. Rev. Lett.*, 92(22):224801, 2004.
- [3] Evgenij L Saldin, Evgeny A Schneidmiller, and Mikhail V Yurkov. Self-amplified spontaneous emission fel with energy-chirped electron beam and its application for generation of attosecond x-ray pulses. *Phys. Rev. ST Accel. Beams*, 9(5):050702, 2006.
- [4] A. Marinelli, E. Hemsing, and J. B. Rosenzweig. Using the relativistic two-stream instability for the generation of soft-x-ray attosecond radiation pulses. *Phys. Rev. Lett.*, 110:064804, Feb 2013.
- [5] D. J. Dunning, B. W. J. McNeil, and N. R. Thompson. Few-cycle pulse generation in an x-ray free-electron laser. *Phys. Rev. Lett.*, 110:104801, Mar 2013.
- [6] H.-C. Wu, J. Meyer-ter Vehn, B. M. Hegelich, and J. C. Fernández. Non-linear coherent thomson scattering from relativistic electron sheets as a means to produce isolated ultrabright attosecond x-ray pulses. *Phys. Rev. ST Accel. Beams*, 14:070702, Jul 2011.
- [7] A. Paz, S. Kuschel, C. Rödel, M. Schnell, O. Jäckel, M. C. Kaluza, and G. G. Paulus. Thomson backscattering from laser-generated, relativistically moving high-density electron layers. *New J. Phys.*, 14:093018, 2012.
- [8] W. Luo, H. B. Zhuo, Y. Y. Ma, Y. M. Song, Z. C. Zhu, T. P. Yu, and M. Y. Yu. Attosecond thomson-scattering x-ray source driven by laser-based electron acceleration. *Appl. Phys. Lett.*, 103(17):174103, 2013.
- [9] Szabolcs Hack, Sándor Varró, and Attila Czirják. Carrier-envelope phase controlled isolated attosecond pulses in the nm wavelength range, based on superradiant nonlinear thomson-backscattering. *ArXiv e-prints*, September 2017.

- [10] G. Sansone, E. Benedetti, F. Calegari, C. Vozzi, L. Avaldi, R. Flammini, L. Poletto, P. Villoresi, C. Altucci, R. Velotta, S. Stagira, S. De Silvestri, and M. Nisoli. Isolated single-cycle attosecond pulses. *Science*, 314(5798):443–446, 2006.
- [11] W. J. Ma, J. H. Bin, H. Y. Wang, M. Yeung, C. Kreuzer, M. Streeter, P. S. Foster, S. Cousens, D. Kiefer, B. Dromey, X. Q. Yan, J. Meyer ter Vehn, M. Zepf, and J. Schreiber. Bright subcycle extreme ultraviolet bursts from a single dense relativistic electron sheet. *Phys. Rev. Lett.*, 113:235002, 2014.
- [12] T. Tanaka. Proposal to generate an isolated monocycle x-ray pulse by counteracting the slippage effect in free-electron lasers. *Phys. Rev. Lett.*, 114:044801, Jan 2015.
- [13] Z. Tibai, Gy. Tóth, M. I. Mechler, J. A. Fülöp, G. Almási, and J. Hebling. Proposal for carrier-envelope-phase stable single-cycle attosecond pulse generation in the extreme-ultraviolet range. *Phys. Rev. Lett.*, 113:104801, Sep 2014.
- [14] Zoltán Tibai, György Tóth, Zsuzsanna Nagy-Csiha, József András Fülöp, Gábor almási, and János Hebling. Investigation of the newly proposed carrier-envelope-phase stable attosecond pulse source. *ArXiv e-prints*, April 2016.
- [15] György Tóth, Zoltán Tibai, Zsuzsanna Nagy-Csiha, Zsuzsanna Márton, Gábor Almási, and János Hebling. Investigation of novel shape-controlled linearly and circularly polarized attosecond pulse sources. *Nucl. Instrum. Methods Phys. Res. B*, 369(Supplement C):2 – 8, 2016. Photon and fast Ion induced Processes in Atoms, Molecules and Nanostructures (PIPAMON).
- [16] W. P. Leemans, B. Nagler, A. J. Gonsalves, Cs. Tóth, K. Nakamura, C. G. R. Geddes, E. Esarey, C. B. Schroeder, and S. M. Hooker. GeV electron beams from a centimetre-scale accelerator. *Nat. Phys.*, 2:696–699, 2006.
- [17] O Lundh, J Lim, C Rechatin, L Ammoura, A Ben-Ismail, X Davoine, G Gallot, J-P Goddet, E Lefebvre, V Malka, and J Faure. Few femtosecond, few kiloampere electron bunch produced by a laser–plasma accelerator. *Nat. Phys.*, 7:219–222, 2011.
- [18] E. Esarey, C. B. Schroeder, and W. P. Leemans. Physics of laser-driven plasma-based electron accelerators. *Rev. Mod. Phys.*, 81:1229–1285, Aug 2009.
- [19] M. E. Couprie, M. Labat, C. Evain, C. Szwaj, S. Bielawski, N. Hubert, C. Benabderrahmane, F. Briquez, L. Chapuis, F. Marteau, M. Valléau, O. Marcouillé, P. Marchand, M. Diop, J. L. Marlats, K. Tavakoli, D. Zerbib, L. Cassinari, F. Bouvet, C. Herbeaux, C. Bourassin-Bouchet, D. Denetière, F. Polack, A. Lestrade, M. Khojyan, W. Yang, G. Sharma, P. Morin, and A. Loulergue. Strategies towards a compact xuv free electron laser adopted for the lunex5 project. *Journal of Modern Optics*, 63(4):309–323, 2016.

- [20] M. C. Hoffmann and J. A. Fülöp. Intense ultrashort terahertz pulses: generation and applications. *J. Phys. D: Appl. Phys.*, 44:083001, 2011.
- [21] H. Hirori, A. Doi, F. Blanchard, and K. Tanaka. Single-cycle terahertz pulses with amplitudes exceeding 1 mv/cm generated by optical rectification in linbo₃. *Appl. Phys. Lett.*, 98:091106, 2011.
- [22] C. Vicario, A. V. Ovchinnikov, S. I. Ashitkov, M. B. Agranat, V. E. Fortov, and C. P. Hauri. Generation of 0.9-mj thz pulses in dstms pumped by a cr:mg₂sio₄ laser. *Appl. Phys. Lett.*, 98:091106, 2011.
- [23] J. A. Fülöp, Z. Ollmann, C. Lombosi, C. Skrobol, S. Klingebiel, L. Pálfalvi, F. Krausz, S. Karsch, and J. Hebling. Efficient generation of thz pulses with 0.4 mj energy. *Opt. Express*, 22(17):20155–20163, 2014.
- [24] T. I. Oh, Y. J. Yoo, Y. S. You, and K. Y. Kim. Generation of strong terahertz fields exceeding 8 mv/cm at 1 khz and real-time beam profiling. *Appl. Phys. Lett.*, 105(4):041103, 2014.
- [25] J. A. Fülöp, Gy. Polónyi, B. Monoszlai, G. Andriukaitis, T. Balciunas, A. Pugzlys, G. Arthur, A. Baltuska, and J. Hebling. Highly efficient scalable monolithic semiconductor terahertz pulse source. *Optica*, 3:1075, 2016.
- [26] Benjamin K. Ofori-Okai, Prasahnt Sivarajah, W. Ronny Huang, and Keith A. Nelson. Thz generation using a reflective stair-step echelon. *Opt. Express*, 24(5):5057–5068, Mar 2016.
- [27] László Pálfalvi, Zoltán Ollmann, Levente Tokodi, and János Hebling. Hybrid tilted-pulse-front excitation scheme for efficient generation of high-energy terahertz pulses. *Opt. Express*, 24(8):8156–8169, 2016.
- [28] László Pálfalvi, György Tóth, Levente Tokodi, Zsuzsanna Márton, József András Fülöp, Gábor Almási, and János Hebling. Numerical investigation of a scalable setup for efficient terahertz generation using a segmented tilted-pulse-front excitation. *Opt. Express*, 25(23), 2017.
- [29] C. Vicario, M. Jazbinsek, A. V. Ovchinnikov, O. V. Chefonov, S. I. Ashitkov, M. B. Agranat, and C. P. Hauri. High efficiency thz generation in dstms, dast and oh1 pumped by cr:forsterite laser. *Opt. Express*, 23(4):4573–4580, Feb 2015.
- [30] J A Fülöp, Zs Major, A Henig, S Kruber, R Weingartner, T Clausnitzer, E-B Kley, A Tünnermann, V Pervak, A Apolonski, J Osterhoff, R Hörlein, F Krausz, and S Karsch. Short-pulse optical parametric chirped-pulse amplification for the generation of high-power few-cycle pulses. *New J. Phys.*, 9:438, 2007.
- [31] Zsuzsanna Major, Sergei A. Trushin, Izhar Ahmad, Mathias Siebold, Christoph Wandt, Sandro Klingebiel, Tie-Jun Wang, József András Fülöp, Andreas Henig, Sebastian Kruber, Raphael Weingartner, Antonia Popp, Jens Osterhoff, Rainer Hörlein, Joachim Hein, Vladimir Pervak, Alexander Apolonski, Ferenc Krausz, and Stefan Karsch. Basic concepts and current status of the petawatt field synthesizer - a new approach to ultrahigh field generation. *Rev. Laser Eng.*, 37(6):431–436, 2009.

- [32] Hanieh Fattahi, Helena G. Barros, Martin Gorjan, Thomas Nubbe-meyer, Bidoor Alsaif, Catherine Y. Teisset, Marcel Schultze, Stephan Prinz, Matthias Haefner, Moritz Ueffing, Ayman Alismail, Lénárd Vámos, Alexander Schwarz, Oleg Pronin, Jonathan Brons, Xiao Tao Geng, Gun-nar Arisholm, Marcelo Ciappina, Vladislav S. Yakovlev, Dong-Eon Kim, Abdallah M. Azzeer, Nicholas Karpowicz, Dirk Sutter, Zsuzsanna Major, Thomas Metzger, and Ferenc Krausz. Third-generation femtosecond tech-nology. *Optica*, 1(1):45–63, Jul 2014.
- [33] S. Gordienko and A. Pukhov. Scalings for ultrarelativistic laser plasmas and quasimonoenergetic electrons. *Phys. Plasmas*, 12:043109, 2005.
- [34] J. D. Jackson. *Classical Electrodynamics*. Wiley, 2007.
- [35] A. D. Debus, M. Bussmann, M. Siebold, A. Jochmann, U. Schramm, T. E. Cowan, and R. Sauerbrey. Traveling-wave thomson scattering and optical undulators for high-yield euv and x-ray sources. *Appl. Phys. B*, 100(1):61–76, Jul 2010.
- [36] J.-C. Diels and W. Rudolph. *Ultrashort Laser Pulse Phenomena*. Elsevier Inc., 2006.
- [37] Eric Esarey, Sally K. Ride, and Phillip Sprangle. Nonlinear thomson scat-tering of intense laser pulses from beams and plasmas. *Phys. Rev. E*, 48(4):3003–3021, 1993.
- [38] Sally K. Ride, Eric Esarey, and Michael Baine. Thomson scattering of intense lasers from electron beams at arbitrary interaction angles. *Phys. Rev. E*, 52:5425–5442, Nov 1995.
- [39] György Tóth, József András Fülöp, and János Hebling. Periodically intensity-modulated pulses by optical parametric amplification for multi-cycle tunable terahertz pulse generation. *Opt. Express*, 25(23), 2017.